Cardiac Fibroblast Activation in Patients Early After Acute Myocardial Infarction: Integration with MR Tissue Characterization and Subsequent Functional Outcome

Johanna Diekmann*[1], Tobias Koenig*[2], James T. Thackeray[1], Thorsten Derlin[1], Christoph Czerner[1,2], Jonas Neuser[2], Tobias L. Ross[1], Andreas Schäfer[2], Jochen Tillmanns[2], Johann Bauersachs*[2], and Frank M. Bengel*[1]

[1]*Department of Nuclear Medicine, Hannover Medical School, Hannover, Germany; and* [2]*Department of Cardiology and Angiology, Hannover Medical School, Hannover, Germany*

After acute myocardial infarction (AMI), fibroblast activation protein (FAP) upregulation exceeds the infarct region. We sought further insights into the physiologic relevance by correlating FAP-targeted PET with tissue characteristics from cardiac MRI (CMR) and functional outcome. **Methods:** Thirty-five patients underwent CMR, perfusion SPECT, and ^{68}Ga-FAP inhibitor (FAPI)-46 PET/CT within 11 d after AMI. Infarct size was determined from SPECT by comparison to a reference database. For PET, regional SUVs and isocontour volumes of interest determined the extent of cardiac FAP upregulation (FAP volume). CMR yielded functional parameters, area of injury (late gadolinium enhancement [LGE]) and T1/T2 mapping. Follow-up was available from echocardiography or CMR after 139.5 d (interquartile range, 80.5–188.25 d) ($n = 14$). **Results:** The area of FAP upregulation was significantly larger than the SPECT perfusion defect size (58% ± 15% vs. 23% ± 17%, $P < 0.001$) and infarct area by LGE (28% ± 11%, $P < 0.001$). FAP volume significantly correlated with CMR parameters at baseline (all $P < 0.001$): infarct area ($r = 0.58$), left ventricle (LV) mass ($r = 0.69$), end-systolic volume ($r = 0.62$), and end-diastolic volume ($r = 0.57$). Segmental analysis revealed FAP upregulation in 308 of 496 myocardial segments (62%). Significant LGE was found in only 56% of FAP-positive segments, elevated T1 in 74%, and elevated T2 in 68%. Fourteen percent (44/308) of FAP-positive segments exhibited neither prolonged T1 or T2 nor significant LGE. Of note, FAP volume correlated only weakly with simultaneously measured LV ejection fraction at baseline ($r = -0.32$, $P = 0.07$), whereas there was a significant inverse correlation with LV ejection fraction obtained at later follow-up ($r = -0.58$, $P = 0.007$). **Conclusion:** Early after AMI and reperfusion therapy, activation of fibroblasts markedly exceeds the hypoperfused infarct region and involves noninfarcted myocardium. The ^{68}Ga-FAPI PET signal does not match regional myocardial tissue characteristics as defined by CMR but is predictive of the evolution of ventricular dysfunction. FAP-targeted imaging may provide a novel biomarker of LV remodeling that is complementary to existing techniques.

Key Words: myocardial infarction; fibroblast activation protein; PET; left ventricular remodeling

J Nucl Med 2022; 63:1415–1423
DOI: 10.2967/jnumed.121.263555

Fibrotic tissue remodeling after injury leads to functional impairment and an adverse outcome in the affected structure or organ. In cardiac disease, myocardial fibrosis contributes to the development and progression of heart failure. Recent evidence has highlighted molecular pathways that activate quiescent cardiac fibroblasts, which have emerged as attractive therapeutic targets to support cardiac repair and mitigate loss of function (*1–4*).

Acute myocardial infarction (AMI) is an important contributor to the development of heart failure (*5*). An immediate and organized inflammatory immune reaction triggers the activation of quiescent fibroblasts (*6,7*). Activated myofibroblasts migrate to injured tissue and contribute to fibrotic scar formation. A sufficient scar is required for adequate repair, but an excessive profibrotic response and involvement of remote myocardium support adverse ventricular remodeling, culminating in progressive contractile dysfunction (*6,8*). Accordingly, whereas fibrosis has emerged as a potential therapeutic target, its double-edged nature after AMI likely requires a personalized approach for medical decision making. Noninvasive, quantitative, fibrosis-targeted imaging may be instrumental for this purpose.

Fibroblast activation protein (FAP) is a membrane-bound serine protease (*2,9*) highly expressed by activated myofibroblasts. Recently, several FAP inhibitors (FAPIs) have been introduced for targeted PET. Initially, ^{68}Ga-FAPI PET was used for imaging of various tumors (*10*), but retrospective analysis of oncologic cohorts established an association between FAP signal and cardiac risk factors, including arterial hypertension and diabetes mellitus (*11*). Increased cardiac signal has also been reported after chemotherapy or chest radiotherapy (*12*). Recently, experimental studies supported the feasibility of ^{68}Ga-FAPI PET to identify fibroblast activation in animal models of AMI (*13,14*). Additionally, clinical reports confirmed a strong ^{68}Ga-FAPI PET signal in patients with AMI—signal that frequently exceeded the nonviable infarct area (*15–17*). Whether this phenomenon is predictive of adverse functional outcome, however, remains unknown. Likewise, the relationship between ^{68}Ga-FAPI PET signal and cardiac MRI (CMR) tissue characteristics is not well defined. CMR identifies late gadolinium enhancement (LGE) in injured regions, and it provides extracellular volume and native T1 and T2 relaxation times as measures of tissue fibrosis (T1) and edema (T2) throughout the entire myocardium (*18*). In contrast to ^{68}Ga-FAPI PET, which identifies a cellular signal from activated myofibroblasts, these CMR-derived parameters reflect mostly extracellular tissue composition.

We hypothesized that ^{68}Ga-FAPI PET reflects a myocardial signal early after AMI that is not identical to CMR-derived tissue

Received Nov. 23, 2021; revision accepted Feb. 17, 2022.
For correspondence or reprints, contact Frank M. Bengel (bengel.frank@mh-hannover.de) or Johanna Diekmann (diekmann.johanna@mh-hannover.de).
*Contributed equally to this work.
Published online Feb. 24, 2022.

characteristics and that predicts later development of ventricular dysfunction. Our hypothesis was tested on a cohort of AMI patients who underwent multiparametric, multimodality noninvasive cardiac imaging early after standard-of-care reperfusion therapy.

MATERIALS AND METHODS

Study Design and Participants

This retrospective single-center study included 35 consecutive patients (30 men, 5 women; mean age ± SD, 57 ± 11 y) who had undergone clinical resting myocardial perfusion SPECT, FAP-targeted PET with ^{68}Ga-FAPI-46, and CMR within 11 d after reperfusion therapy for AMI at Hannover Medical School. All subjects had been treated by percutaneous coronary intervention and stenting within 4 ± 3 h of symptom onset and received dual-antiplatelet therapy. All had ST-segment elevation, absence of a prior history of AMI or coronary intervention or other cardiac procedures, success of reperfusion immediately after angioplasty, absence of systemic immunologic or infectious or profibrotic disease, and availability of complete imaging datasets, clinical records, and laboratory parameters. Clinical characteristics and medication at the time of imaging are summarized in Table 1. Routinely recorded laboratory values, as determined by standard Hannover Medical School clinical procedures, included peak creatine kinase as a

TABLE 1
Characteristics of the 35 Patients

Variable	Characteristic	Data
Age (y)		57 ± 11
Sex	Female	5/35 (14.3)
	Male	30/35 (85.7)
Height (cm)		178 ± 7
Weight (kg)		86.8 ± 15.8
Cardiovascular risk factors	Diabetes	11/35 (31.4)
	Arterial hypertension	19/35 (54.3)
	Dyslipidemia	25/35 (71.4)
	Obesity (BMI > 30 kg/m^2)	9/35 (25.7)
	Smoking	21/35 (60.0)
Culprit vessel	LAD	24/35 (68.6)
	LCX	3/35 (8.6)
	RCA	8/35 (22.9)
Symptom to wire time (min)		234 ± 190
Peak creatine kinase (U/L)		3416 ± 3104
Peak C-reactive protein (mg/L)		42.6 ± 53.2
Peak leukocyte count (1,000/mm^3)		14.4 ± 4.4
Peak creatinine (mg/dL)		97.1 ± 20.7
Medication at PET	ASS	32/35 (91.4)
	P2Y12 antagonists	35/35 (100)
	OAK	3/35 (8.5)
	Statins	35/35 (100)
	β-blockers	33/35 (94.3)
	Noninsulin glucose-lowering drugs	11/35 (31.4)
	Insulin	2/35 (5.7)
	ACE inhibitors	22/35 (62.9)
	ATII blockers	13/35 (37.1)

BMI = body mass index; LAD = left anterior descending coronary artery; LCX = left circumflex coronary artery; RCA = right coronary artery; ASS = aspirin; P2Y12 = the adenosine diphosphate receptor on platelets; OAK = oral anticoagulation; ACE = angiotensin-converting enzyme; ATII = angiotensin 2.

Qualitative data are number and percentage; continuous data are mean ± SD.

TABLE 2
CMR Data for the 35 Patients

Global function parameters	Mean ± SD	Range
LVM (g)	132.6 ± 27.4	87–183
EDV (mL)	144.5 ± 35.5	79–206
ESV (mL)	79.9 ± 25.0	40–139
SV (mL)	64.7 ± 20.1	25–105
LVEF (%)	45.1 ± 9.6	23–64
LGE (mL)	39.9 ± 19.0	0.8–87
LGE (% of ventricle)	28.3 ± 11.2	0.7–49
MO (%)	1.0 ± 1.2	0–5.2

LVM = LV mass; EDV = end-diastolic volume; ESV = end-systolic volume; SV = stroke volume; MO = microvascular obstruction.

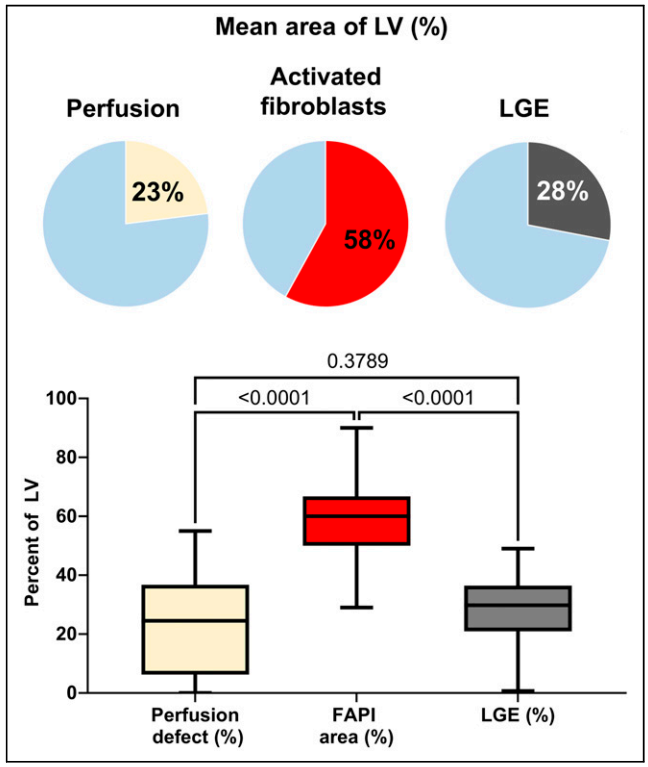

FIGURE 1. Box plot of perfusion defect size (yellow), activated fibroblasts (red), and LGE (gray) in entire patient group, expressed as percentage of LV. Bars are mean with range.

marker of myocardial injury, and C-reactive protein and leukocyte count as markers of systemic inflammatory response. The institutional review board approved the project (approval 9553_BO_K_2021), and all subjects signed a consent form.

Radionuclide Imaging

At 5.0 ± 1.5 d after AMI (median, 5.0; range, 3–8 d), resting myocardial perfusion SPECT was performed to determine the success of reperfusion, using 388 ± 32 MBq of ^{99m}Tc-tetrofosmin and a dedicated cardiac camera (Discovery 530c; GE Healthcare). Infarct size was determined using commercially available software for polar map generation (4DM; Invia) and a local reference database for comparison.

FAP-targeted PET was conducted at 7.5 ± 1.3 d (range, 5–11 d) using the specific ligand ^{68}Ga-FAPI-46, which was synthesized in-house by good manufacturing practices as previously described (*19*) and used clinically according to §13.2b of the German Pharmaceuticals Act, for determination of myocardial injury. Static PET images were acquired for 20 min using a Biograph mCT 128 PET/CT system (Siemens), beginning 60 min after intravenous injection of 114 ± 22 MBq of ^{68}Ga-FAPI-46. Low-dose CT was used for attenuation correction. Images were iteratively reconstructed, using time-of-flight and point-spread-function information (True X; Siemens). SUV_{peak} and SUV_{mean} were obtained for infarct, remote myocardium, blood pool (left atrium), and other organs using volumes of interest of 1 cm^3 and commercial software (syngo.via, V50B; Siemens Healthcare). Cardiac FAP volume was determined by an isocontour volume of interest including all voxels above an individual threshold (blood pool SUV_{mean} +2 SDs). We set this threshold because of lack of an established alternative standard. Additionally, the area of FAP upregulation was calculated by polar map analysis, using the same threshold, as previously described (*15*). Mean segmental SUV was calculated using the AHA 17-segment model and polar maps.

CMR

CMR was performed using a 1.5-T scanner (Magnetom Avanto; Siemens) in 33 of 35 patients (94%) at 4 ± 2 d after AMI (median, 4; range, 2–10 d). Cine images were obtained using a balanced steady-state free-precession sequence (True FISP; Siemens). Parametric T1 and T2 maps were acquired in 3 short-axis slices (basal, midventricular, and apical left ventricle [LV] covering 16 segments [available for 31 patients]). T1 mapping was performed using the modified look-locker inversion recovery sequence before (native) and after administration of contrast agent. Quantitative balanced steady-state free-procession–based T2 maps (True FISP) were acquired in corresponding short-axis slices. The upper threshold of normal T1 was defined as 1,023 ms and T2 as 60 ms according to our clinical standard (*20,21*). LGE was imaged by phase-sensitive inversion recovery sequences, 10–15 min after injection of a 0.15 mmol/kg bolus of gadolinium-diethylenetriaminepentaacetic acid (gadobutrol; Bayer Healthcare). Extracellular volume fraction was calculated by measurement of myocardial and blood T1 relaxation times before and after administration of contrast agent and using hematocrit value. Global analysis included determination of LV ejection fraction (LVEF), volumes, mass, extent of LGE, and microvascular obstruction. Segmental analysis included wall thickening, native T1 and T2 relaxation times, and extracellular volume fraction, using the 16-segment model. cvi42 software (Circle Cardiovascular Imaging) was used.

Follow-up LV Function

In 14 of 35 patients (40%), follow-up LVEF was available from standardized in-house echocardiography (biplane Simpson method, n = 12) or repeat cine CMR (n = 2), at a mean of 133 ± 63 d (median, 140 d; range, 42–214 d) after AMI.

Statistical Analysis

Statistical analyses were performed using SPSS, version 27, and GraphPad Prism, version 9. Categoric variables are presented with absolute and relative frequencies. For quantitative continuous variables, testing of gaussian distribution was performed using Shapiro–Wilk tests. For data with a gaussian distribution, paired Student t tests or 1-way ANOVA with Tukey multiple-comparison tests were used. Nonparametric unpaired data were analyzed with Mann–Whitney U tests. Pearson correlation coefficients were calculated for bivariate correlation analyses. All statistical analyses were performed 2-sided, and a P value of less than 0.05 indicated statistical significance.

RESULTS

FAP Signal Exceeds the Infarct Region and Correlates with Blood Markers of Tissue Damage and Inflammation

The perfusion defect size in SPECT was 23% ± 17% of the LV, ranging from 0% to 55%. In 7 of 35 (20.0%) patients, complete

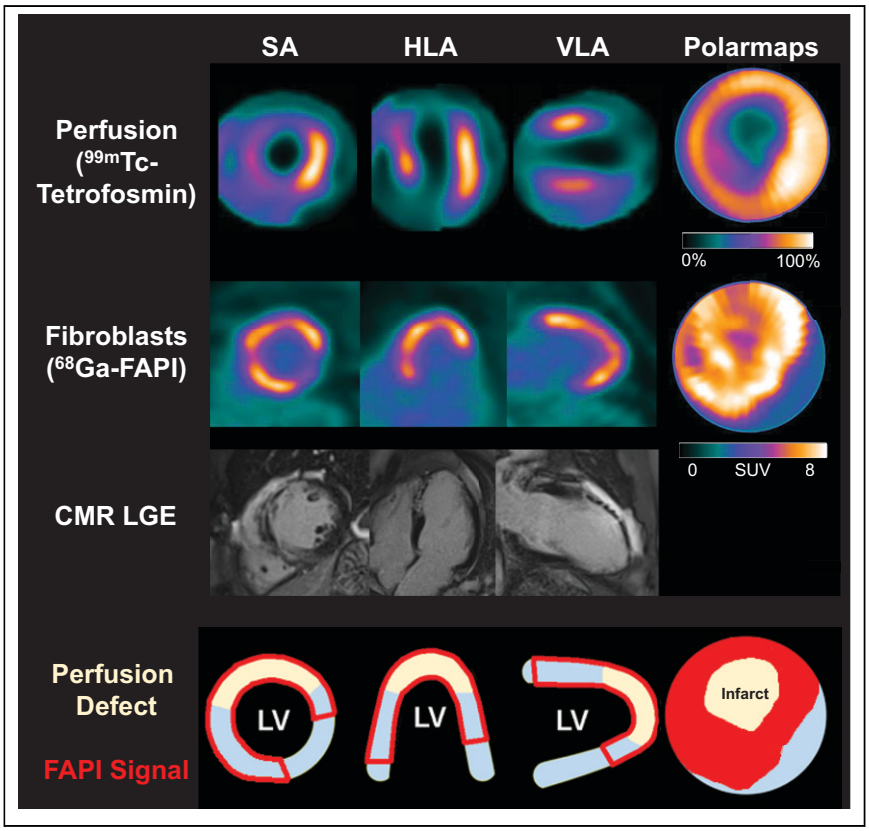

FIGURE 2. Myocardial perfusion images using ^{99m}Tc-tetrofosmin at rest, ^{68}Ga-FAPI PET, LGE from CMR, and schematic drawings of LV. Area of fibroblast activation as indicated by ^{68}Ga-FAPI-46 PET signal exceeds infarct area and LGE signal, the most common type of myocardial FAP distribution. HLA = horizontal long axis; SA = short axis; VLA = vertical long axis.

reperfusion was documented by absence of a significant perfusion defect. Myocardial injury as measured by LGE volume comprised 40 ± 19 mL, or 28% ± 11% of the LV (range, 1%–49%), and correlated with perfusion defect size (r = 0.646, P < 0.001). Other CMR-derived global parameters are summarized in Table 2.

^{68}Ga-FAPI PET showed a significantly elevated signal in the territory of the culprit infarct vessel (SUV_{peak}, 6.4 ± 1.5) in all patients. PET imaging ranged from 5 to 11 d after AMI, and no significant relationship between myocardial FAP volume and time after AMI was detected within this interval (Spearman ρ: r = 0.056, P = 0.750). Consistent with prior reports, most patients showed markedly increased areas of elevated FAP signal when compared with either the SPECT perfusion defect (58% ± 15% vs. 23% ± 17%, P < 0.001) or the extent of myocardial injury measured by LGE (28% ± 11%, P < 0.001; Figs. 1 and 2). Even among the 7 patients with complete reperfusion and absence of a SPECT perfusion defect, an elevated FAP signal was consistently detected in the affected coronary territory (Fig. 3). Low amounts of LGE were detected in patients without a residual SPECT perfusion defect; however, LGE was less prominent than in other patients (13.7% ± 9.8% vs. 31.5% ± 8.8%, P < 0.001), and FAP signal was significantly greater (54.7% ± 19.4%, P < 0.001). Only 3 of 35 patients had a difference between FAP area and an infarct size of less than 15%, all of whom exhibited large perfusion defects (Fig. 4). The area of FAP upregulation correlated with perfusion defect size (r = 0.407, P = 0.015) and LGE (r = 0.344, P = 0.050), suggesting that larger infarcts also lead to larger amounts of replacement fibrosis. However, the mismatch area between FAP area and perfusion defect size as a marker of viable myocardium with activated fibroblasts inversely correlated with perfusion defect size (r = −0.622, P < 0.001). The specific number of days after AMI at which imaging was performed in this study did not have a significant effect on differences between CMR, perfusion, and ^{68}Ga-FAPI PET patterns. Further results of ^{68}Ga-FAPI PET are summarized in Table 3. Only 2 patients presented with small amounts of microvascular obstruction (<5%). At 69% (24/35), the left anterior descending coronary artery was the most frequent culprit vessel (Table 1). FAP area was larger than in the other coronary territories (left anterior descending coronary artery, 64.8 ± 12.6, vs. left circumflex coronary artery, 41.0 ± 13.8, vs. right coronary artery, 44.1 ± 8.7; P (ANOVA) < 0.001), but mismatch between FAP area and perfusion defect size did not show significant differences among coronary territories.

Signal in remote myocardium and other regions (liver, spleen, bone marrow, and lung) was low and did not correlate with infarct signal. Significant correlations were detected between FAP volume and maximum creatine kinase (r = 0.42, P = 0.012) as well as inflammatory markers (maximum C-reactive protein: r = 0.43, P = 0.010; maximum white blood cell count: r = 0.31, P = 0.07). Diabetes mellitus was associated with a larger FAP volume (134 ± 53 cm^3 vs. 93 ± 36 cm^3 for patients without diabetes, P = 0.012), whereas other cardiovascular risk factors were not associated with FAP signal.

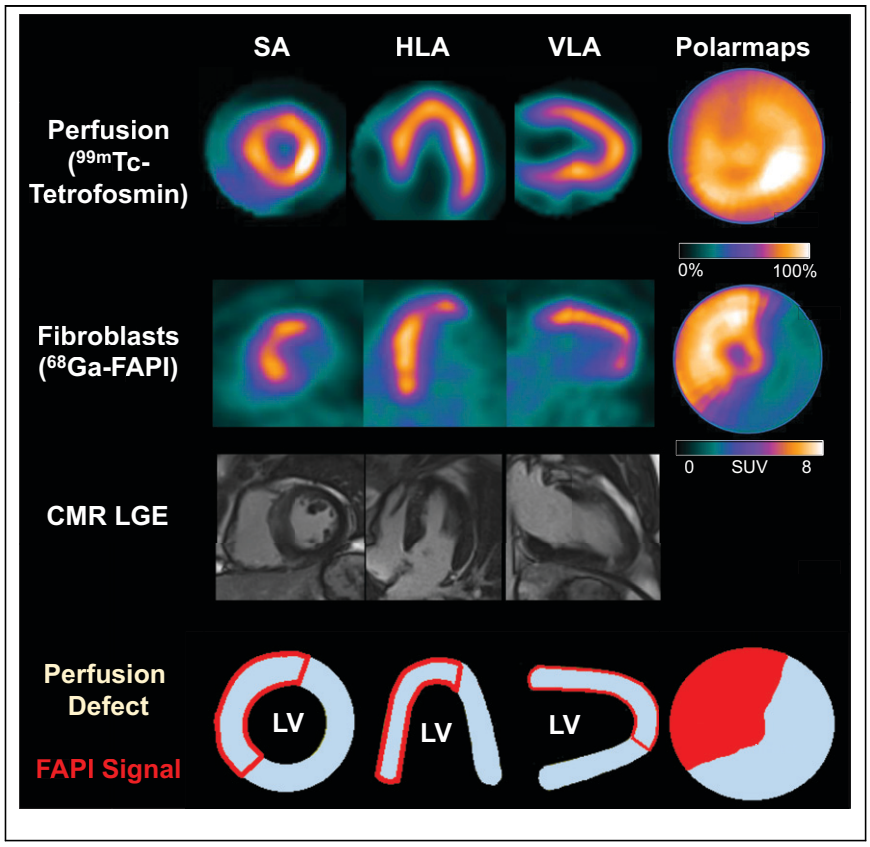

FIGURE 3. Myocardial perfusion images using ^{99m}Tc-tetrofosmin at rest, ^{68}Ga-FAPI PET, LGE from CMR, and schematic drawings of LV. No relevant perfusion defect is seen after AMI, because of complete reperfusion, and there is no significant LGE, but large area of fibroblast activation is seen. HLA = horizontal long axis; SA = short axis; VLA = vertical long axis.

FAP Signal Does Not Match Regional CMR Tissue Characteristic Segmental Analysis

For segmental correlation with CMR, apex was excluded from studies, leaving 16 segments per patient and a total of 496 segments (CMR T1 and T2 mapping available in 31 patients). Overall, the segmental mean FAP signal correlated with LGE extent (r = 0.660, P < 0.001), T1 and T2 relaxation times (r = 0.485, P < 0.001, and r = 0.475, P < 0.001, respectively), and extracellular volume (r = 0.557, P < 0.001). But there were marked differences when classifying segments as positive or negative for the respective tissue parameter (Fig. 5): 308 of 496 (64%) segments were classified as FAP-positive, using blood pool SUV_{mean} + 2 SDs as a threshold (*15*). A transmural LGE signal of more than 25% was present in 172 of 308 segments (56%). A prolonged T1 relaxation time above 1,023 ms (*22*), a threshold indicative of tissue fibrosis, was present in 227 of 308 segments (74%). A prolonged T2 relaxation time longer than 60 ms (*21*), consistent with edema, was present in 210 of 308 segments (68%). Of note, 44 of 308 (14%) FAP-positive segments had normal T1 and T2 relaxation and no relevant LGE. This confirms that FAP signal frequently

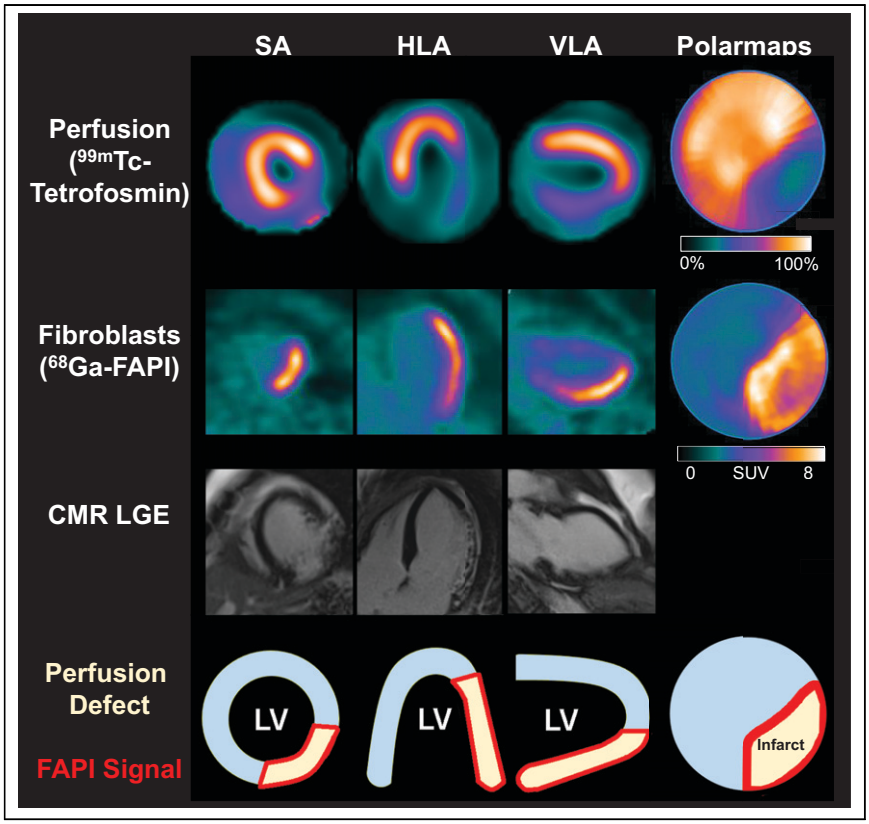

FIGURE 4. Myocardial perfusion images using ^{99m}Tc-tetrofosmin at rest, ^{68}Ga-FAPI PET, LGE from CMR, and schematic drawings of LV. Fibroblast activation only marginally exceeds infarct region. HLA = horizontal long axis; SA = short axis; VLA = vertical long axis.

FAP-Positive Segments Present with Impaired Contractility

Segmental SUV_{mean} (496 segments) showed a mild but significant inverse correlation with segmental wall thickening ($r = -0.224$, $P < 0.001$). When 3 subgroups of segments were compared, normally perfused segments without FAP signal had significantly greater wall thickening than normally perfused segments with elevated FAP signal, whereas wall thickening was least in hypoperfused segments, all of which had an elevated FAP signal (Fig. 6).

FAP Signal Correlates with Ventricular Geometry and Functional Outcome

At baseline, FAP volume significantly correlated with LV mass ($r = 0.69$, $P > 0.001$), end-diastolic volume ($r = 0.57$, $P > 0.001$), end-systolic volume ($r = 0.62$, $P > 0.001$), and LGE volume ($r = 0.58$, $P > 0.001$). A trend to correlation was detected between FAP volume and initial LVEF ($r = -0.32$, $P = 0.07$). Interestingly, FAP volume showed a stronger, significant correlation with LVEF at follow-up ($r = -0.583$, $P = 0.007$; Fig. 7). Among patients with complete follow-up, those with at least 1 FAP-positive but T1-, T2-, and LGE-negative segment ($n = 6$) had a lower follow-up LVEF than those without such segments ($n = 6$; 47% ± 8% vs. 57% ± 3%, $P = 0.02$). Overall, this finding suggests that a higher number of activated fibroblasts early after AMI is associated with more severe LV dysfunction in the subsequent chronic stage after AMI.

extends beyond areas that are abnormal at CMR tissue characterization. Only few FAP segments showed LGE or altered T1 and T2 relaxation times. In these segments, LGE most likely reflects chronic stages of preexisting scar, potentially due to cardiovascular comorbidities. Furthermore, elevated signal in T1 and T2 mapping in the absence of FAP signal may identify segments with edema but no fibroblast activity.

DISCUSSION

Our results confirm that regional upregulation of FAP by activated fibroblasts yields a very high contrast between the injured

TABLE 3
Radionuclide Imaging Data

	All patients (n = 35)		CMR available (n = 33)	
Variable	Mean ± SD	Range	Mean ± SD	Range
Perfusion defect (SPECT % of polar map)	23.2 ± 17.4	0–55	23.6 ± 17.4	0–55
PET signal (^{68}Ga-FAPI-46 SUV_{peak})				
Spleen	1.43 ± 0.40	0.96–2.61	1.43 ± 0.41	0.96–2.61
Liver	1.50 ± 0.47	0.82–2.93	1.48 ± 0.47	0.82–2.93
Bone marrow	1.05 ± 0.29	0.61–2.04	1.05 ± 0.29	0.61–2.04
Lungs	0.82 ± 0.32	0.34–2.17	0.81 ± 0.33	0.34–2.17
Blood pool (left atrium)	1.97 ± 0.40	1.32–3.21	1.97 ± 0.40	1.32–3.21
Remote myocardium	1.41 ± 0.38	0.91–2.84	1.41 ± 0.39	0.91–2.84
Infarct	6.41 ± 1.53	3.52–10.60	6.54 ± 1.46	4.24–10.60
Area of FAP upregulation (% of polar map)	58.0 ± 15.4	29–90	57.7 ± 15.8	29–90
Volume of FAP signal (cm^3)	105.8 ± 45.6	33.6–215.4	105.9 ± 46.6	33.6–215.4

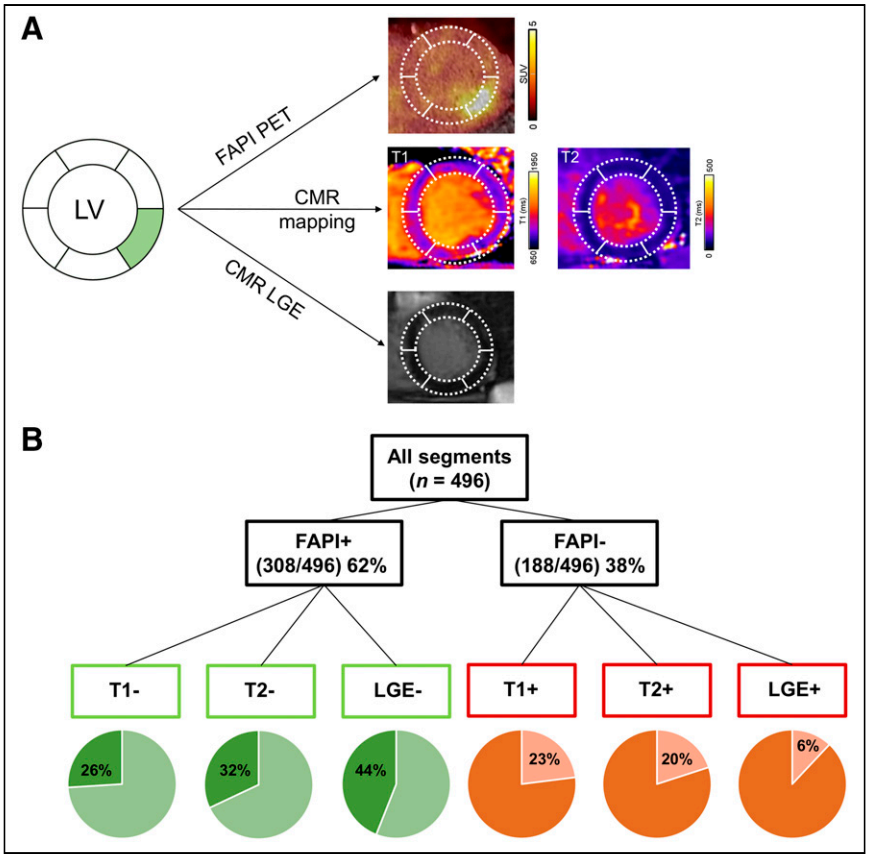

FIGURE 5. (A) Patient example with FAP-positive, T1-negative, T2-negative, and LGE-negative segment. (B) Segmental comparison of myocardial ^{68}Ga-FAPI-46 distribution, native T1 and T2 mapping, and LGE from CMR, using 16-segment model (apex excluded) in 31 AMI patients with complete datasets, resulting in total of 496 segments.

infarct and periinfarct region and unaffected remote myocardium, blood pool, and surrounding structures. FAP upregulation markedly exceeds the infarct region in patients early after AMI and standard-of-care reperfusion therapy. This result is consistent with the notion that FAP upregulation plays a role not only in replacement fibrosis in the primary injured region but also in reactive fibrosis that may compromise noninfarcted myocardium (*15,23*). Our observation of a link between extent of early FAP signal and LV dysfunction at later follow-up lends further support to this concept. Our results suggest that the FAPI signal is a multifactorial parameter that integrates a variety of influencing factors in the commonly heterogeneous clinical setting of patients early after AMI. Yet, the association with functional outcome makes the parameter intriguing for further exploration.

Integrative multimodal segmental analysis provides further insights into the relationship between fibroblast activation and extracellular tissue composition. Interestingly, the mismatch between FAP area and perfusion defect size was larger when infarct size was smaller. Speculatively, larger amounts of myocardial salvage and reperfusion injury may contribute to this elevated FAP signal as a potential precursor of interstitial fibrosis. Future studies may provide further insights into these interrelations. Although we found that FAP upregulation grossly correlated with CMR tissue parameters, there were relevant regional discordances. A significant fraction of FAP-positive segments not only exhibited absent LGE but also lacked prolongation of T1 and T2 relaxation times on CMR. This finding is of particular interest because it suggests that the results of ^{68}Ga-FAPI PET are not interchangeable with CMR tissue characteristics. Rather, ^{68}Ga-FAPI PET may add further, biologically distinct, information. Currently, LGE imaging is well established for detection of focal, mostly replacement fibrosis after myocardial injury in ischemia, inflammation, or cardiomyopathy. But cardiac pathologies, including diffuse, mostly interstitial alterations such as fibrosis or edema, cannot be quantified adequately by LGE (*24*). For this purpose, CMR mapping techniques that quantitatively determine tissue relaxation times for T1 (prolonged, for example, in interstitial fibrosis and infiltration) and T2 (primarily reflecting water content and prolonged in edema and inflammation) have been successfully designed. These parameters are increasingly applied in clinics (*25*) and provide information about the extent and composition of extracellular space. Myocardial fibrosis is commonly defined as an expansion of the cardiac interstitium by deposition of extracellular matrix proteins such as collagen. But modern concepts of the pathogenesis of fibrosis increasingly emphasize the role of cellular components, for which there is a tight interplay between functionally diverse subsets of fibroblasts, extracellular matrix composition, and regulation by the immune system (*26*). ^{68}Ga-FAPI PET identifies the cellular component of this process by specifically visualizing expression of FAP on activated myofibroblasts (*9,13,14*). Our results suggest that this profibrotic cellular signal is abundant in the territory of the infarct vessel early after AMI, that it may be present in myocardial segments that do not yet show elevated T1 relaxation as a measure of interstitial protein deposition, and that it may be present in segments that still do not show elevated T2 as a measure of edema. Speculatively, elevated FAP signal is an early and abundant fibroblast response after reperfusion and its immediate inflammatory reaction. The cellular FAP signal may then precede the subsequent deposition of extracellular matrix that establishes overt fibrosis. Clearly, further work is needed to elucidate the relative time course of the cellular, PET-derived signal and the interstitial, CMR-derived signal, along with their importance for functional outcome and for guidance of therapeutic interventions. In this regard, it should be noted that PET with other, immune cell–targeted, tracers may also identify the cellular component of inflammation, for integration with fibrosis-targeted imaging (*27,28*).

Regional patterns in our AMI patients suggest that the area of FAP upregulation may be interlinked with the ischemic area at risk. Prior SPECT studies have shown the feasibility of area-at-risk assessment using perfusion imaging after radiotracer injection before and after reperfusion of AMI (*29*). Yet, this logistically demanding approach is not broadly feasible and has not been available in our setting. In CMR, area at risk has been proposed to be estimated via quantity of edema in T2-weighted images, but preclinical histologic validation delivered partly inconclusive

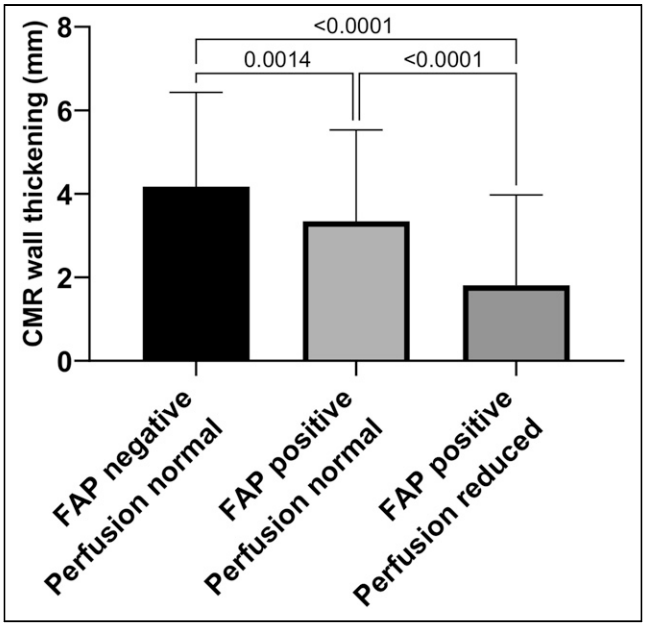

FIGURE 6. Three groups for analysis of wall thickening and contractility: FAP-negative and normally perfused segments representing remote myocardium, FAP-positive but normally perfused segments representing border zone, and FAP-positive segments with reduced perfusion representing core infarct zone. Wall thickening was significantly impaired in all FAP-positive segments with or without reduced perfusion (infarct and border zones).

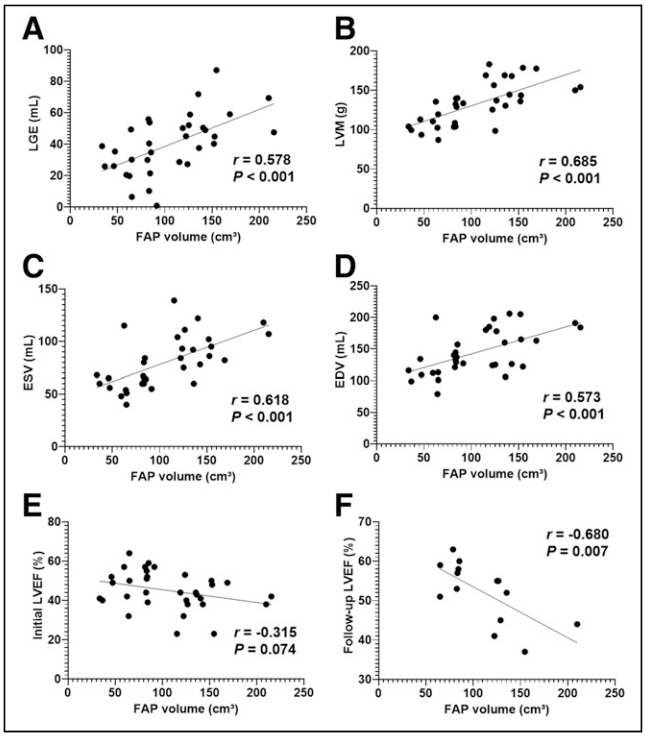

FIGURE 7. Correlation between global myocardial FAP volume early after AMI and synchronously measured markers of cardiac geometry and function from CMR. (A–D) Volume of LGE (mL) (A), LV mass (LVM; g) (B), end-systolic volume (ESV; mL) (C), and end-diastolic volume (EDV; mL) (D). (E and F) Nonsignificant trend to correlation with LVEF at baseline (E), and significant correlation with follow-up LVEF (F).

results on colocalization of edema and area at risk (*30*). In our study, FAP signal partly colocalized with detected edema in T2-weighted images. Interestingly, the mismatch of FAP area and perfusion defect size was larger when infarct size was smaller, suggesting a relationship with successful reperfusion. FAP-positive segments also showed impaired wall thickening both in the infarct and in the border zone, where it may reflect regional postischemic stunning. And last, the detected correlation of FAP uptake with levels of creatine kinase suggest an association between number of activated fibroblasts and ischemia/reperfusion ischemic injury. Ultimately, the relationship between area of fibroblast activation and area at risk warrants further investigation. Inclusion of myocardial perfusion imaging after tracer injection before revascularization, or the addition of stress perfusion imaging for flow reserve measurements, may be helpful in this regard in the future.

The long-term importance of imaging the myofibroblast component of profibrotic activity will depend on its predictive value for subsequent LV remodeling and heart failure progression. Our results show that the area of fibroblast activation at the time of PET imaging was associated with the extent of injury and geometric features such as the mass and volume of the LV, whereas the relation with contractile function was less pronounced initially. This relationship, however, changed at follow-up in the chronic post-AMI stage, when a larger extent of FAP signal early after AMI was associated with more severe contractile dysfunction. Notably, we even observed a lower mean follow-up LVEF in patients with a FAP-positive but CMR-negative tissue signal early after AMI. This might be a first indicator supporting an independent relevance of myocardial FAP signal for functional outcome; however, follow-up of LV function was available in only 14 patients. A larger prospective work will be needed to confirm these results.

We also observed a larger extent of myocardial fibroblast activation in a subgroup of patients with diabetes mellitus, whereas no differences were found analyzing other cardiovascular risk factors (age, sex, arterial hypertension, hyperlipidemia, smoking, and obesity). This finding was independent of infarct size. In AMI, diabetes mellitus is associated with elevated long-term mortality (*31,32*). Also, it has been shown that patients with adult-onset diabetes may exhibit extensive perivascular, interstitial, and even replacement fibrosis, in the absence of hypertension or coronary artery disease (*33*). The molecular mechanisms responsible for the contribution of diabetes mellitus to cardiac fibrosis remain poorly understood (*34*). Whether a more pronounced fibroblast activation in response to ischemic hypoperfusion plays a role in the adverse outcome of diabetic patients is another hypothesis generated by our preliminary observation that should be tested in subsequent studies.

A strong FAP signal was measured in the affected region, whereas signal from remote myocardium and other regions (liver, spleen, bone marrow, and lungs) was much lower. This supports the feasibility of FAP-targeted imaging to guide antifibrotic therapeutic strategies. Importantly, it also supports the feasibility of FAP-targeted therapies themselves, which may modulate and attenuate profibrotic activity if administered precisely in suitable individuals and at the right time (*3*). In the future, molecular imaging using FAPI ligands might help us to understand mechanisms and select patients for individual treatment using advanced antifibrotic measures.

Some limitations of our work should be considered. The sample size was small, and the analysis was retrospective, leading to even

smaller samples for follow-up. No serial imaging was performed, and the time course of the FAP signal after AMI remains incompletely defined. We chose to use a threshold for detection of FAP-positive myocardial areas because of absence of an established standard. This approach was pursued as a best possible approach in the absence of validated alternatives. Other measures such as the SUV or segmental analyses were threshold-independent and confirm the major conclusions of our work. Our work should be seen as hypothesis-generating for further studies, which may aim at identifying the optimal time point for imaging FAP expression to predict the progression of postinfarct remodeling most effectively. Further work may also focus on defining the incremental value of FAP-targeted imaging over standard clinical risk markers, CMR, and other molecular targeted approaches such as imaging of the inflammatory response to injury (*35*). The outcome sample of this study was too small for meaningful multivariate analyses. Finally, matching of PET and CMR results may not have been perfect because studies were obtained on separate camera systems on different days. We also cannot completely discount possible variation of imaging parameters over time in this study, although we sought to minimize effects by performing imaging on 3 consecutive days, when possible. PET signal was significantly elevated in the infarct region and in the periinfarct region, where wall thickening was impaired as a consequence of ischemic injury. Partial-volume effects were considered minor therefore, and in the absence of established methods, no correction for partial-volume effects was applied. In the future, hybrid PET/MRI systems may offer simultaneous acquisition of CMR and PET parameters of myocardial repair after AMI (*36*).

CONCLUSION

Taken together, this work provides new insights into the regional pattern of fibroblast activation early after AMI. The area of elevated FAP signal reaches beyond the injured infarct region and may even involve regions without prolonged T1 or T2 relaxation as CMR markers of interstitial fibrosis, infiltration, or edema. This suggests that the cell-based signal of fibroblast activation is distinct from CMR-derived interstitial characteristics and may be complementary. Importantly, the early FAP signal was associated with a subsequent impairment of LV function, suggesting that it may be a predictor of adverse LV remodeling.

DISCLOSURE

This work was supported by the Deutsche Forschungsgemeinschaft (DFG, Clinical Research Unit KFO 311: Johann Bauersachs and Frank Bengel; Clinician Scientist Program PRACTIS: Johanna Diekmann), the Leducq Foundation (Transatlantic Network "Immunofib HF": Frank Bengel, James Thackeray, and Johanna Diekmann), and "REBIRTH—Research Center for Translational Regenerative Medicine" (State of Lower Saxony: James Thackeray, Johann Bauersachs, and Frank Bengel). No other potential conflict of interest relevant to this article was reported.

ACKNOWLEDGMENT

Precursor for ^{68}Ga-FAPI-46 was kindly provided by Uwe Haberkorn, MD, University of Heidelberg.

KEY POINTS

QUESTION: Does myocardial fibroblast activation early after AMI correlate with CMR tissue characteristics, and is it predictive of subsequent development of ventricular dysfunction?

PERTINENT FINDINGS: Thirty-five patients underwent ^{68}Ga-FAPI-46 PET and CMR within 11 d after reperfusion therapy for AMI. The region of fibroblast activation on ^{68}Ga-FAPI PET extended beyond the fibrotic scar. Also, there were segmental discrepancies between FAPI signal and T1 and T2 relaxation times from CMR. FAPI signal early after AMI correlated with reduced LVEF in the subsequent chronic stage.

IMPLICATIONS FOR PATIENT CARE: ^{68}Ga-FAPI PET may be complementary to CMR and serve as an independent marker of the risk of adverse cardiac remodeling after AMI.

REFERENCES

1. Travers JG, Kamal FA, Robbins J, Yutzey KE, Blaxall BC. Cardiac fibrosis: the fibroblast awakens. *Circ Res.* 2016;118:1021–1040.
2. Furtado MB, Nim HT, Boyd SE, Rosenthal NA. View from the heart: cardiac fibroblasts in development, scarring and regeneration. *Development.* 2016;143:387–397.
3. Aghajanian H, Kimura T, Rurik JG, et al. Targeting cardiac fibrosis with engineered T cells. *Nature.* 2019;573:430–433.
4. Gourdie RG, Dimmeler S, Kohl P. Novel therapeutic strategies targeting fibroblasts and fibrosis in heart disease. *Nat Rev Drug Discov.* 2016;15:620–638.
5. Conrad N, Judge A, Tran J, et al. Temporal trends and patterns in heart failure incidence: a population-based study of 4 million individuals. *Lancet.* 2018;391:572–580.
6. Prabhu SD, Frangogiannis NG. The biological basis for cardiac repair after myocardial infarction: from inflammation to fibrosis. *Circ Res.* 2016;119:91–112.
7. Lafuse WP, Wozniak DJ, Rajaram MVS. Role of cardiac macrophages on cardiac inflammation, fibrosis and tissue repair. *Cells.* 2020;10:51.
8. Sutton MG, Sharpe N. Left ventricular remodeling after myocardial infarction: pathophysiology and therapy. *Circulation.* 2000;101:2981–2988.
9. Tillmanns J, Hoffmann D, Habbaba Y, et al. Fibroblast activation protein alpha expression identifies activated fibroblasts after myocardial infarction. *J Mol Cell Cardiol.* 2015;87:194–203.
10. Kratochwil C, Flechsig P, Lindner T, et al. ^{68}Ga-FAPI PET/CT: tracer uptake in 28 different kinds of cancer. *J Nucl Med.* 2019;60:801–805.
11. Siebermair J, Kohler MI, Kupusovic J, et al. Cardiac fibroblast activation detected by Ga-68 FAPI PET imaging as a potential novel biomarker of cardiac injury/remodeling. *J Nucl Cardiol.* 2021;28:812–821.
12. Heckmann MB, Reinhardt F, Finke D, et al. Relationship between cardiac fibroblast activation protein activity by positron emission tomography and cardiovascular disease. *Circ Cardiovasc Imaging.* 2020;13:e010628.
13. Varasteh Z, Mohanta S, Robu S, et al. Molecular imaging of fibroblast activity after myocardial infarction using a ^{68}Ga-labeled fibroblast activation protein inhibitor, FAPI-04. *J Nucl Med.* 2019;60:1743–1749.
14. Langer LBN, Hess A, Korkmaz Z, et al. Molecular imaging of fibroblast activation protein after myocardial infarction using the novel radiotracer [^{68}Ga]MHLL1. *Theranostics.* 2021;11:7755–7766.
15. Diekmann J, Koenig T, Zwadlo C, et al. Molecular imaging identifies fibroblast activation beyond the infarct region after acute myocardial infarction. *J Am Coll Cardiol.* 2021;77:1835–1837.
16. Kessler L, Kupusovic J, Ferdinandus J, et al. Visualization of fibroblast activation after myocardial infarction using ^{68}Ga-FAPI PET. *Clin Nucl Med.* 2021;46:807–813.
17. Notohamiprodjo S, Nekolla SG, Robu S, et al. Imaging of cardiac fibroblast activation in a patient after acute myocardial infarction using ^{68}Ga-FAPI-04. *J Nucl Cardiol.* April 15, 2021 [Epub ahead of print].
18. González A, Schelbert EB, Diez J, Butler J. Myocardial interstitial fibrosis in heart failure: biological and translational perspectives. *J Am Coll Cardiol.* 2018;71:1696–1706.
19. Loktev A, Lindner T, Burger EM, et al. Development of fibroblast activation protein-targeted radiotracers with improved tumor retention. *J Nucl Med.* 2019;60:1421–1429.

20. Goebel J, Seifert I, Nensa F, et al. Can native T1 mapping differentiate between healthy and diffuse diseased myocardium in clinical routine cardiac MR imaging? *PLoS One.* 2016;11:e0155591.
21. Verhaert D, Thavendiranathan P, Giri S, et al. Direct T2 quantification of myocardial edema in acute ischemic injury. *JACC Cardiovasc Imaging.* 2011;4:269–278.
22. Rosmini S, Bulluck H, Captur G, et al. Myocardial native T1 and extracellular volume with healthy ageing and gender. *Eur Heart J Cardiovasc Imaging.* 2018;19:615–621.
23. Nagaraju CK, Dries E, Popovic N, et al. Global fibroblast activation throughout the left ventricle but localized fibrosis after myocardial infarction. *Sci Rep.* 2017;7:10801.
24. Salerno M, Kramer CM. Advances in parametric mapping with CMR imaging. *JACC Cardiovasc Imaging.* 2013;6:806–822.
25. Messroghli DR, Moon JC, Ferreira VM, et al. Clinical recommendations for cardiovascular magnetic resonance mapping of T1, T2, T2* and extracellular volume: a consensus statement by the Society for Cardiovascular Magnetic Resonance (SCMR) endorsed by the European Association for Cardiovascular Imaging (EACVI). *J Cardiovasc Magn Reson.* 2017;19:75.
26. Humeres C, Frangogiannis NG. Fibroblasts in the infarcted, remodeling, and failing heart. *JACC Basic Transl Sci.* 2019;4:449–467.
27. Hess A, Thackeray JT, Wollert KC, Bengel FM. Radionuclide image-guided repair of the heart. *JACC Cardiovasc Imaging.* 2020;13:2415–2429.
28. Glasenapp A, Derlin K, Gutberlet M, et al. Molecular imaging of inflammation and fibrosis in pressure overload heart failure. *Circ Res.* 2021;129:369–382.
29. Matsunari I, Schricke U, Bengel FM, et al. Extent of cardiac sympathetic neuronal damage is determined by the area of ischemia in patients with acute coronary syndromes. *Circulation.* 2000;101:2579–2585.
30. Beijnink CWH, van der Hoeven NW, Konijnenberg LSF, et al. Cardiac MRI to visualize myocardial damage after ST-segment elevation myocardial infarction: a review of its histologic validation. *Radiology.* 2021;301:4–18.
31. Gholap NN, Achana FA, Davies MJ, Ray KK, Gray L, Khunti K. Long-term mortality after acute myocardial infarction among individuals with and without diabetes: a systematic review and meta-analysis of studies in the post-reperfusion era. *Diabetes Obes Metab.* 2017;19:364–374.
32. Johansson S, Rosengren A, Young K, Jennings E. Mortality and morbidity trends after the first year in survivors of acute myocardial infarction: a systematic review. *BMC Cardiovasc Disord.* 2017;17:53.
33. Regan TJ, Lyons MM, Ahmed SS, et al. Evidence for cardiomyopathy in familial diabetes mellitus. *J Clin Invest.* 1977;60:884–899.
34. Russo I, Frangogiannis NG. Diabetes-associated cardiac fibrosis: cellular effectors, molecular mechanisms and therapeutic opportunities. *J Mol Cell Cardiol.* 2016;90:84–93.
35. Werner RA, Koenig T, Diekmann J, et al. CXCR4-targeted imaging of post-infarct myocardial tissue inflammation: prognostic value after reperfused myocardial infarction. *JACC Cardiovasc Imaging.* 2022;15:372–374.
36. Abgral R, Dweck MR, Trivieri MG, et al. Clinical utility of combined FDG-PET/MR to assess myocardial disease. *JACC Cardiovasc Imaging.* 2017;10:594–597.